THE JOURNAL OF PHYSICAL CHEMISTRY C

Article

pubs.acs.org/JPCC

Computational Study of Ga NMR Shielding in Metallic Gallides

Robert Laskowski,*[,†] Khoong Hong Khoo,[†] Frank Haarmann,[‡,§] and Peter Blaha[∥]

[†]Institute of High Performance Computing, A*STAR, 1 Fusionopolis Way, #16-16, Connexis 138632, Singapore

[‡]Max-Planck-Institut für Chemische Physik fester Stoffe, Nöthnitzer Straße 40, 01187 Dresden, Germany

[§]Institut für Anorganische Chemie (IAC), RWTH-Aachen, Landoltweg 1. 52074 Aachen, Germany

[∥]Institute of Materials Chemistry, Vienna University of Technology, Getreidemarkt 9/165-TC, A-1060 Vienna, Austria

ABSTRACT: We present first-principles calculations of the isotropic NMR Ga shielding in metallic MGa_2 with M = Ca, Sr, Ba and MGa_4 with M = Na, Ca, Sr and Ba. We show that the experimentally observed trend of Ga NMR shifts is as expected driven mainly by the spin part of the response, but the orbital contribution must not be neglected. For all analyzed compounds the spin contact term constitute the major component of the response, except for $BaGa_2$, where the spin-dipolar contribution is unusually large. This spin-dipolar contribution is related to the difference of the Ga-4p_z and 4$p_{x,y}$ partial density of states (PDOS) at the Fermi level, which is large only for $BaGa_2$. It is related to the honeycomb-like Ga-lattice and the distances between Ga atoms. The spin-contact term is determined to a large extend by Ga-4s PDOS at the Fermi level, because the magnetic field leads to a small spin-splitting and a reoccupation of spin-up and spin-down states. This Ga-4s PDOS is related to the local atomic structure around the Ga atoms and results in fact from an overlap with the neighboring Ga-4p orbitals, therefore more symmetric local arrangements of atoms around Ga result in higher Ga-4s PDOS. However, we noticed that for very low Ga-4s PDOS the spin contact term does not tend to zero but changes sign and becomes diamagnetic. This can be explained by the energy dependence of the Ga-4s radial wave function near the nucleus, leading to a contraction/expansion of 4s densities, respectively. This effect is also present in all insulating materials; however, it has been neglected so far in literature.

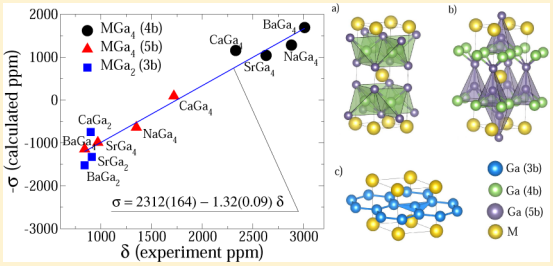

INTRODUCTION

First-principles calculations of NMR shielding for insulating solids are now relatively easy and routinely carried out to aid the interpretation of measured spectra.[1−3] Such calculations are much more complicated for metallic systems and therefore less common. In this case, the nuclear spin interacts not only with the electron orbit but also with its spin. So far only shieldings for metallic elements have been computed.[4,5] The difficulty is, however, not related to the more complicated nature of the screening of the nuclear spin, but mainly to technical issues like slow convergence of the shielding with respect to the Brillouin zone sampling and the sensitivity to the approach applied to determine the occupancy of the electronic states close to the Fermi level.[5] If these facts are carefully considered, reliable parameters can be computed.

In this work we focus on computing the isotropic shielding at the Ga nucleus in intermetallic MGa_2, with M = Ca, Sr, Ba, and MGa_4, with M = Na, Ca, Sr and Ba compounds. Ga, residing near the Zintl border in the Periodic Table of Elements, forms compounds with electropositive elements characterized by attractive Ga−Ga interactions with short Ga−Ga contacts, as proposed by the Zintl concept.[6] They possess metallic conductivity. The Ga local atomic structure and the number of Ga−Ga contacts interlinking the Ga atoms proves to be quite flexible. The degree of the interlinking increases with Ga content. For instance, isolated Ga atoms are found in $Ca_{28}Ga_{11}$,[7] 2- or 3-fold bonded Ga clusters are observed in Sr_8Ga_7 or Ba_8Ga_7.[8] 3-fold coordinated Ga atoms, forming two-dimensional networks, are seen in various MGa_2,[9] whereas 4- and 5-fold bonded atoms and three-dimensional interlinking are characteristic in MGa_4.[10] To reflect this flexibility, Ga atoms are referred to as Ga(3b), Ga(4b), and Ga(5b), indicating 3-, 4-, and 5-fold coordination. Here, the term bonded is not used in the sense of two-electron−two-center bonds, but describe interatomic distances that are smaller than the average Ga−Ga distance in elemental *a*-Ga (2.70 Å).[11] MGa_4, with M = Na, Sr, and Ba, crystallizes in the $BaAl_4$ structure (Table 1), with one Ga(4b) and one Ga(5b) site, shown in Figure 1a,b. The Ga(4b) sites are coordinated by four equidistant Ga(5b), forming a distorted tetrahedron with two angles slightly different from ideal tetrahedral 109.5°. The Ga(5b) local atomic structure is a pyramid with a square base of Ga(4b) and a Ga(5b) at the top. The atomic structure of $CaGa_4$ is a monoclinic distortion of the $BaAl_4$ type.[12] For the Ga(4b) site the four Ga(5b) are not equidistant but slightly split into two shorter and two longer distances. MGa_2 crystallize in the AlB_2-type structure with a 2D honeycomb-like Ga layer shown in Figure 1c. The layer is flat showing some corrugation for $CaGa_2$.[13] Considering the different interatomic distances within and between the layers,

Received: November 8, 2016
Published: December 9, 2016

DOI: 10.1021/acs.jpcc.6b11210
J. Phys. Chem. C 2017, 121, 753−760

Table 1. Structural Parameters[9,10,33] for MGa_4 and MGa_2[a]

	$NaGa_4$	$CaGa_4$	$SrGa_4$	$BaGa_4$
lattice	*I*4/*mmm*	*C*2/*m*	*I*4/*mmm*	*I*4/*mmm*
a	4.226	6.181	4.447	4.566
b		6.248		
c	11.228	6.130	10.745	10.775
γ		121.036		
d[Ga(4b)−Ga(5b)]	2.626	2.584	2.643	2.675
		2.651		
d[Ga(5b)−Ga(5b)]	2.497	2.478	2.514	2.598
∠[Ga(5b),Ga(4b),Ga(5b)]	110.8	112.3	114.5	117.2
	106.8	107.5	107.0	105.8
∠[Ga(4b),Ga(5b),Ga(4b)]	69.1	72.5	73.0	74.2
	$CaGa_2$	$SrGa_2$	$BaGa_2$	
lattice	*P*63/*mmc*	*P*6/*mmm*	*P*6/*mmm*	
	4.4627	4.3484	4.4322	
	7.3640	4.7360	5.0824	
Ga−Ga	2.650	2.511	2.559	
corrugation	0.621			

[a]In the lattice section, we show *a*, *b*, *c* (in Å), and *γ* for $CaGa_4$, and only *a* and *c* for the rest of tetragallides. d[Ga(4b)−Ga(5b)] and d[Ga(5b)−Ga(5b)] stands for distance between Ga atoms. ∠[Ga(5b),Ga(4b),Ga(5b)] represent the angles between Ga(4b)−Ga(5b) bonds on Ga(4b) local atomic structure (see Figure 1a), ∠[Ga(4b),Ga(5b),Ga(4b)] stands for the angle between Ga(5b)−Ga(4b) in Ga(5b) local structure (Figure 1b). For $CaGa_2$ the corrugation (in Å) of the Ga layer is given, which is zero for the rest of the digallides.

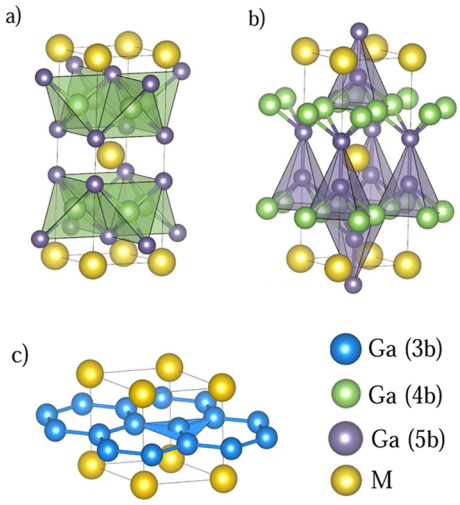

Figure 1. Local atomic structure for (a) Ga(4b) in MGa_4, (b) Ga(5b) in MGa_4, and (c) Ga(3b) in MGa_2.[14]

the Ga atoms are 3 + 1-fold coordinated leading to Ga(3b+1b) in $CaGa_2$.

NMR spectroscopy is sensitive to the local arrangements of atoms and their bonding situations. However, the relation between the NMR parameters and the structure is, in general, not well understood in solids. This is particularly the case for metals. Considering both the flexibility of Ga forming various local structures and the metallic character, the intermetallic gallides present a valuable opportunity for studying such relations. In this paper we compute spin and orbital components of the isotropic shielding for Ga in various di- and tetragallides. We discuss the relation between the spin component of the shielding and the atomic structure, which determines to a large extent the trends of the measured NMR signal shifts.

EXPERIMENTALLY ACCESSIBLE NMR PARAMETERS

Line shape analysis is usually performed to determine the experimental coupling parameters of solid state NMR signals. This attempt describes the shape of the signals with phenomenological parameters being related to the various interactions. For ^{71,69}Ga with $I = 3/2$, the signal is often dominated by the so-called quadrupole coupling resulting from the interaction of the nuclear quadrupole moment and the surrounding charge distribution.[9,10,15,16] The latter is described by the electric field gradient (EFG) with its main principal axis V_{ZZ} and the asymmetry parameter η_Q.

While the isotropic NMR signal shift influences only the position of the signal the anisotropic NMR signal shift has some impact on the line shape of the signal. Both the isotropic and the anisotropic signal shift can be derived by careful data analysis. For low symmetry sites, also, the relative orientation of the principal axis systems of both quadrupole coupling and shift interactions can be determined by analysis of field-dependent experiments.[17]

Two main contributions to the NMR signal shift have to be distinguished. These are the chemical shift (δ) resulting from the orbital motions of the electrons and the Knight shift ($\mathcal{K}$).[18−21] The latter is due to the interaction of the nuclear magnetic moment with the spins of electrons in metallic materials. Since $\mathcal{K}$ and δ cannot be experimentally separated, the complete shift parameters Δ_{iso}, Δ_{aniso}, and η_Δ seem to be appropriate to emphasize the various contributions.[22] The complete isotropic signal shift of metallic materials is given by

$$\Delta_{iso} = \delta_{iso} + \mathcal{K}_{iso} \quad (1)$$

To obtain further insights into the atomistic origin of the NMR coupling parameters theoretical investigations have to be performed.

DOI: 10.1021/acs.jpcc.6b11210
J. Phys. Chem. C 2017, 121, 753−760

DETAILS OF THE COMPUTATIONAL APPROACH

The NMR shielding $\vec{\sigma}$ tensor describes a response of a system to an external magnetic field. It is defined as a proportionality between the induced magnetic field $\mathbf{B}_{ind}$ at the nucleus at site $\mathbf{R}$ and the external uniform field $\mathbf{B}$:

$$\mathbf{B}_{ind}(\mathbf{R}) = -\vec{\sigma}(\mathbf{R})\mathbf{B} \tag{2}$$

It can be measured only with respect to a reference compound, as a $\delta(\mathbf{R}) = \sigma_{ref} - \sigma(\mathbf{R})$, and often only its isotropic part $\sigma(\mathbf{R}) = \mathrm{Tr}[\vec{\sigma}(\mathbf{R})]$ is known.

The external magnetic field is a relatively weak perturbation compared to the typical energy scale of the electronic structure, therefore, its effect on the spin and orbit of an electron can be separated in the theoretical calculations. The orbital part of the shielding, that is, orbital component of the induced field $\mathbf{B}_{ind}$ is obtained directly from the Biot-Savart law (in atomic units, with c as speed of light):

$$\mathbf{B}_{ind}(\mathbf{R}) = \frac{1}{c}\int d^3r\,\mathbf{j}(\mathbf{r}) \times \frac{\mathbf{R}-\mathbf{r}}{|\mathbf{r}-\mathbf{R}|^3} \tag{3}$$

where $\mathbf{j}(\mathbf{r})$ is the induced orbital current. The method for computing $\mathbf{j}(\mathbf{r})$ is based on a linear response approach[23−25] originally developed by Mauri, Pfrommer, and Louie (MPL).[23] It has been adapted and implemented within the all-electron, full potential augmented plane wave (APW) WIEN2k code.[26,27] The details of the implementation are described in our previous publications.[28,29] Formally our approach belongs to a set of gauge transformation methods, often referred to as IGCV (individual gauge for core and valence) with a "$d(r) = r$" gauge choice for the valence electrons.[30]

In order to compute the induced spin density and the spin part of the NMR shielding tensor we use a direct approach,[5] instead of applying the linear response formalism proposed for instance in ref 4. We perform self-consistent spin polarized calculations with a finite external magnetic field ($\mathbf{B}_{ext}$) acting on the electron spin only. The interaction with the external field can be cast into a spin-dependent potential leading to a spin splitting of eigenstates and a finite spin magnetization. It does not break the symmetry of the solid and therefore such calculations are straightforward. The induced magnetic field at a given nucleus is computed using an expression for the magnetic hyperfine field:[31]

$$\mathbf{B}_{hf} = \frac{8\pi}{3}\mathbf{m}_{av} + \int \frac{S(r)}{r^3}[3(\mathbf{m}(r)\hat{r})\hat{r} - \mathbf{m}(r)]\,d^3r \tag{4}$$

where the first term is the Fermi contact term (B_c), and the second captures the spin-dipolar contribution (B_{sd}) to the hyperfine field. The spin contribution (σ_s), for example, the Knight shift ($\mathcal{K}$) to the shielding is then simply given by two terms:

$$\sigma_s = \sigma_c + \sigma_{sd} = -B_c/B_{ext} - B_{sd}/B_{ext} \tag{5}$$

The Fermi contact term (σ_c) is related to the average spin density ($m_{av}(r) = \rho_{up}(r) - \rho_{dn}(r)$) in a region near the nucleus with a diameter equal to the Thomson radius.[31] The value of the spin-dipolar component (σ_{sd}) comes almost entirely from within the atomic sphere, which simplifies the calculations. The details and benchmarks of our approach can be found in ref 5. In order to obtain a sizable response and evaluate the NMR shielding with a numerical precision at the level of 1 ppm we apply in our calculations a field B_{ext} of 100 T, which induces a spin-splitting of approximately 1 mRy. We have checked the linearity of the induced field with respect to the external field.

Within the APW method the unit cell is decomposed into nonoverlapping atomic spheres and an interstitial region. The unperturbed wave functions as well as their first order perturbations are expressed using plane waves augmented with an atomic like angular momentum expansion inside the atomic spheres S_α:

$$\Psi_{n,\mathbf{k}}(\mathbf{r}) = \begin{cases} \frac{1}{\sqrt{\Omega}}\sum_{\mathbf{G}} C_G^{n,\mathbf{k}} e^{i(\mathbf{G}+\mathbf{k})\cdot\mathbf{r}}, & \mathbf{r}\in I \\ \sum_{lm} W_{lm}^{n,\alpha,\mathbf{k}}(r)Y_{lm}(\hat{r}), & \mathbf{r}\in S_\alpha \end{cases} \tag{6}$$

Inside the atomic spheres APW uses numerical radial functions $W_{lm}^{n,\alpha,\mathbf{k}}(r)$ computed at predefined linearization energies,[26] which are chosen to match the energies of the corresponding occupied bands. This approach yields basically the exact radial wave functions for the occupied and shallow conduction band states. However, it is not a complete basis and not well suited to expand the perturbation of the wave function due to an external magnetic field. To remedy this problem, we supply eight additional local orbitals (NMR-LO) for $l \le 3$, with radial wave functions evaluated at higher energies,[28] set such that an additional radial node is introduced for each NMR-LO. Moreover, we augment the perturbed wave function with radial functions proportional to $r\frac{\partial}{\partial r}u(r)$ (DUDR).[29] This makes the method basically numerically exact within a given DFT functional.[29] Besides that the NMR calculations within our APW method do not require any other computational parameters considerably different from generally accepted defaults. For the sake of analysis we keep the atomic sphere radii for Ga atoms constant at 2.3 au. The plane wave cut off K_{max} for the APW basis set is determined by $RK_{max} = 8.0$, where R represents the smallest atomic radius in a calculation. The Brillouin zone was sampled with a regular mesh of up to 10^6 k-points for the spin component of the NMR shielding and 0.512×10^6 for its orbital part. The calculations have been carried out with the Perdew, Burke, Ernzerhof (PBE)[32] version of the generalized gradient approximation (GGA) to the DFT exchange-correlation functional.

The internal atomic positions have been optimized; however, we kept the experimental lattice parameters.[9,10,33] The basic structural parameters are listed in Table 1. For MGa_4, both Ga(4b)−Ga(5b) and Ga(5b)−Ga(5b) distances scale roughly with the atomic number of M. $CaGa_4$ may be seen as a slight exception: it crystallizes in spacegroup $C2/m$ instead of $I4/mmm$ and has a deformed tetrahedral Ga(4b) environment with two different Ga(4b)−Ga(5b) distances. For all compounds, the Ga(5b)−Ga(5b) distance is shorter than Ga(5b)−Ga(4b) by roughly 0.1 Å. For MGa_2, the Ga(3b)−Ga(3b) distance increases between $SrGa_2$ and $BaGa_2$. $CaGa_2$ crystallizess in a lover symmetry structure with considerably puckered Ga nets. Within these nets it possesses the largest Ga−Ga distances in the MGa_2 group. The distances between the layers are about 14% larger.[13] As we will show later, the difference in the coordination numbers for the Ga(3b), Ga(3b+1b), Ga(4b), and Ga(5b) sites, as well as small differences in interatomic distances influence the corresponding NMR shielding.

DOI: 10.1021/acs.jpcc.6b11210
J. Phys. Chem. C 2017, 121, 753−760

Table 2. Calculated NMR Isotropic Shielding (σ) and the Decomposition into Orbital Component (σ_o), Spin Contact (σ_c), and Spin Dipolar (σ_{sd}) Terms Computed with a Fermi Smearing of 2 mRy[a]

	site	σ_o (ppm)		σ_c (ppm)		σ_{sd} (ppm)		σ (ppm)
$NaGa_4$	(4b)	1534	(0,3)	−2800	(−3,25)	−12	(1,0)	−1278
	(5b)	1136	(2,3)	−602	(−4,2)	115	(1,1)	647
$CaGa_4$	(4b)	1407	(1,−12)	−2577	(5,−17)	14	(1,1)	−1151
	(5b)	1283	(6,−3)	−1327	(9,−8)	−43	(1,−2)	−84
$SrGa_4$	(4b)	1304	(7,−12)	−2322	(8,120)	−16	(1,1)	−1034
	(5b)	1142	(22,−5)	−213	(3,49)	64	(0,4)	993
$BaGa_4$	(4b)	1203	(2,−6)	−2796	(10,19)	−84	(1,10)	−1677
	(5b)	1191	(6,−5)	−35	(1,15)	−3	(1,−2)	1153
$CaGa_2$	(3b)	1292	(3,2)	−509	(1,−5)	−14	(1,−3)	769
$SrGa_2$	(3b)	956	(16,22)	475	(−4,8)	−179	(1,7)	1252
$BaGa_2$	(3b)	999	(20,10)	1746	(4,245)	−1166	(1,−227)	1579

[a]The first number in the parentheses represent the change when comparing results with N_k and $N_k/2$ k-points, where N_k is 10^6 and 0.512×10^6 (in full BZ) for spin and orbital components, respectively. The second number in parentheses is the slope (ppm/mRy) describing the dependence of the shielding on the Fermi "smearing", defined as $[\sigma(2\text{ mRy}) - \sigma(4\text{ mRy})]/2\text{mRy}$, where $\sigma(T)$ is the shielding computed with Fermi smearing T.

RESULTS AND DISCUSSION

The calculated NMR shielding and its decomposition into orbital components, spin contact and dipolar terms for the Ga sites are listed in Table 2. We have noticed that for some cases ($SrGa_4$, $BaGa_2$) the dependence of the calculated shielding parameters on the Fermi broadening parameter is very large. The numbers quoted in Table 2 are computed with a small value of k_{BT} = 2 mRy (close to room temperature) and 10^6 k-points for the spin component and 0.512×10^6 for its orbital part (corresponding to full BZ). In addition, we show in parentheses the parameters quantifying the dependency with respect to the Fermi-level smearing and the uncertainty related to k-point convergence (the change when reducing the k-mesh by a factor of 1/2). Most values are converged within a few ppm; only $BaGa_2$ needed special care, because the Fermi energy coincides with a sharp peak in the DOS (see Figure 4). Fortunately, the huge and nonlinear dependency of σ_c and σ_{sd} on the smearing parameter cancels almost completely and σ_s is fairly independent of it.

Figure 2 compares the calculated shielding and the measured isotropic shifts.[9,10] The theoretical and measured values correlate reasonably well, however, using a linear regression, the slope of 1.32 is considerably different from the ideal 1.0. The constant coefficient of the linear regression is equal to −2312 ppm. The standard errors for slope and constant are equal to 0.09 and 164 ppm, respectively. The deviation of the slope from the ideal 1.0 value is one of the shortcomings of DFT[34] related to the band gap problem, at least for insulating materials, where the GGA computed slopes are higher than 1.0. It has been observed that the Becke-Johnson DFT potential[35] usually leads to much improved results;[1,34] however, this method is not applicable to metallic systems. The orbital component (σ_o) shows a relatively weak variation within the set of compounds, as shown in Figure 2a. We see a slightly negative value of the correlation coefficient (−0.14), which partially counteracts the trend of the spin component. According to our experience related to calculations for other systems (unpublished at the moment), this seems to be a quite general feature. Since the spin and orbital component of the experimental shifts cannot be separated, it is not possible to identify which one is responsible for the "slope problem" in this case. The difference in σ_o between the two sites Ga(4b) and Ga(5b) in MGa_4 reaches 400 ppm for $NaGa_4$ and drops to less than 10 ppm for $BaGa_4$. The orbital shift at the Ga(5b) sites shows a much

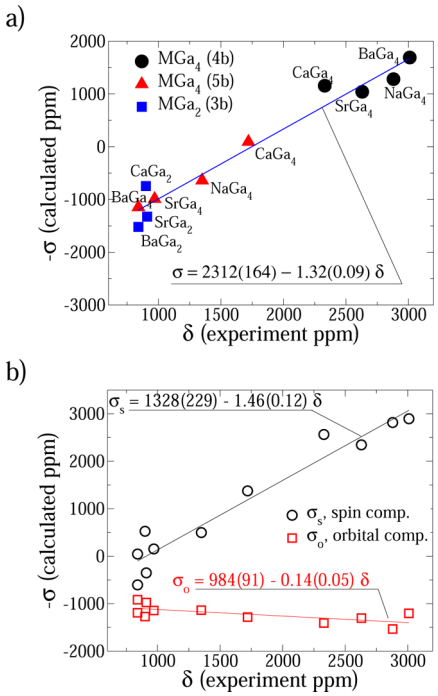

Figure 2. (a) Comparison of calculated shielding (σ) and measured shifts (δ). (b) Correlation of the orbital (σ_o) and spin (σ_s) components of the shielding with the measured shifts. The standard errors for the slope and constant of the linear regression are given in parentheses.

smaller variation of roughly 100 ppm, while σ_o for the Ga(4b) sites varies by more than 300 ppm. For MGa_2, σ_o varies within a range of 350 ppm. This is compatible with measured Ga shifts in insulators, which range from about −700 to 700 ppm.[36] At this point, we confirm previous suggestions[10] that the experimentally observed trend arises mainly due to the spin part of the response. In this case, the Fermi contact term is clearly the major component for most compounds. There is one exception, namely, $BaGa_2$, which has an unusually large spin-dipolar part reaching as much as −1166 ppm, while in all other compounds $|\sigma_{sd}|$ is less than 200 ppm and often even much smaller. We will discuss and explain this later.

The spin contact term is usually interpreted as a result of an induced spin density at the nucleus due to the external

DOI: 10.1021/acs.jpcc.6b11210
J. Phys. Chem. C 2017, 121, 753−760

magnetic field. The magnetic field shifts spin up and down bands in opposite directions in energy scale leading to a larger spin up occupation compared to spin down. Therefore, it is reasonable to assume a paramagnetic (negative) character of such a response with some scaling related to the Ga-s character of the partial density of states (PDOS) at the Fermi level ϵ_F.[37] Interestingly, for $SrGa_2$ and $BaGa_2$, the value of σ_c is positive, which cannot be explained within this simple picture. Let us emphasize that in all cases considered here the contributions to σ_c come predominantly from the valence Ga-4s electrons and the core-polarization is small (in contrast to some transition metals, where the induced 3d moment results in a huge diamagnetic core polarization[5]). In order to understand the origin of the diamagnetic character of the contact term σ_c for $SrGa_2$ and $BaGa_2$, let us consider the spin magnetization density induced by the external magnetic field given by the difference:

$$m(\mathbf{r}) = \psi_\uparrow(\mathbf{r})\psi_\uparrow^*(\mathbf{r}) - \psi_\downarrow(\mathbf{r})\psi_\downarrow^*(\mathbf{r}) \quad (7)$$

where $\psi_\uparrow$ and $\psi_\downarrow$ are wave functions of the spin up and spin down eigenstates. As shown in eq 4, the contact term is related to the average spin density within the Thomson radius; therefore, in order to calculate it, we need to consider only the spherical component of the wave function $\psi_\sigma = 1/\sqrt{4\pi}\,u_\sigma$, where u_σ is a radial function associated with orbital quantum number $l = 0$. The dependency of the radial functions u_σ on the external field can be expressed within first order:

$$u_\sigma(B_{ext}, r) = u^0(r) + \dot{u}^0(r)\Delta\epsilon_\sigma(B_{ext}) \quad (8)$$

where $\Delta\epsilon_\sigma = -\sigma\mu_B B_{ext}$. $u_\sigma^0(r)$ is calculated without the external field B_{ext}, and $\dot{u}_\sigma^0(r)$ is its energy derivative. Therefore, within first order in B_{ext}, the induced magnetization is equal to

$$\mathbf{m}(r) = -\mu_B B[u^0(r)\dot{u}^0(r)] \quad (9)$$

Close to the nucleus, both $u^0(r)$ and $\dot{u}^0(r)$ are positive, as shown in Figure 3, leading to a diamagnetic response. In a case

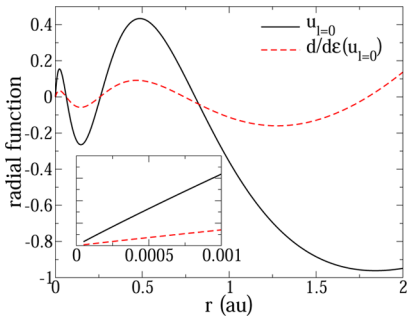

Figure 3. Radial function for Ga 4s in the valence band ($u_{l=0}(r)$) and its energy derivative ($\frac{d}{d\epsilon}u_{l=0}$).

where the Ga s-PDOS at the Fermi level is very small, the paramagnetic component of the contact term may not be large enough to compensate this diamagnetic part. This is observed in Figure 4a, where the correlation between σ_c and the Ga-s PDOS(ϵ_F) is shown for the discussed di- and tetragallides. A first estimate of the diamagnetic component σ_c^{dia} can be obtained from the constant coefficient of the linear regression, which is positive and quite large (950 ppm). However, it is obviously not always constant as both, $SrGa_2$ and $BaGa_2$ have the same very low s-PDOS but very different σ_c. A better estimate of the diamagnetic component of σ_c can be obtained

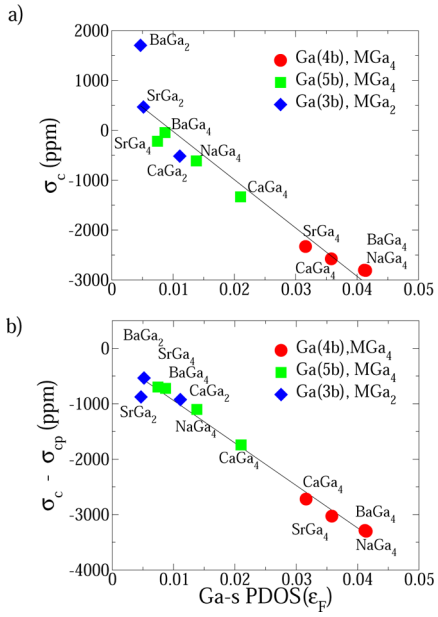

Figure 4. (a) Correlation of the calculated spin part of the shielding (σ_c) with the value of the s partial DOS at ϵ_F. (b) Correlation plotted for its paramagnetic component (σ_c^{para}) resulting from reoccupation of the spin up and down states.

by performing calculations of σ_c constraining the total spin magnetization to zero. Such calculations are done non-self-consistently using the converged eigenstates from the unconstrained calculation with the external magnetic field. In this "fixed-spin-moment"[38] (FSM) calculation, we simply populate the spin up and down eigenstates such that the correct total charge but zero total spin moment are achieved. This results in two different Fermi levels for spin up and down eigenstates, respectively. The values of this estimate of the diamagnetic contribution σ_c^{dia} and the subsequent decomposition of the total contact term $\sigma_c = \sigma_c^{dia} + \sigma_c^{para}$ are displayed in Table 3. The diamagnetic component (σ_c^{dia}) ranges from 400 to 700 ppm for most of the compounds, but $SrGa_2$ and $BaGa_2$ have much larger values of 1010 and 2622 ppm, respectively. This comes probably because of the large induced Ga-4p moment, which introduces an additional diamagnetic 4s response. In principle, only the paramagnetic term σ_c^{para} results from reoccupation of

Table 3. Decomposition of the Spin Contact Component of the Shielding (σ_c) into Its Diamagnetic Component (σ_c^{dia}) Related to the Contraction of the Wave Function and the Paramagnetic Part (σ_c^{para}) Coming from the Reoccupation of the Spin up and down States in the External Magnetic Field

	site	σ_c (ppm)	σ_c^{dia} (ppm)	σ_c^{para} (ppm)
$NaGa_4$	(4b)	−2800	483	−3286
	(5b)	−602	497	−1099
$CaGa_4$	(4b)	−2577	451	−3028
	(5b)	−1327	416	−1743
$SrGa_4$	(4b)	−2322	390	−2720
	(5b)	−213	482	−698
$BaGa_4$	(4b)	−2796	495	−3302
	(5b)	−35	685	−721
$CaGa_2$	(3b)	−509	415	−924
$SrGa_2$	(3b)	475	1010	−535
$BaGa_2$	(3b)	1746	2622	−876

DOI: 10.1021/acs.jpcc.6b11210
J. Phys. Chem. C 2017, 121, 753−760

the spin up and down states in the external magnetic field, and thus, only this term is expected to be directly related to the value of the Ga s-PDOS at Fermi level. In fact, in Figure 4b, the correlation between σ_c^{para} and the Ga s-PDOS is nearly perfectly linear and the constant of the regression is close to zero (−174 ppm).

Let us emphasisze as a side remark that there is no reason why such effects should not be present also for insulating compounds. The contribution to the shielding scales with the energy dependence of the radial function and the amount of charge carried by the spherical part of the valence wave functions. For instance, this contact term ranges from 17 ppm in the very ionic GaF_3 (with a PBE band gap close to 5.2 eV) to 30−100 ppm in semiconductors like GaN or GaSb, which is quite a significant number compared to the precision of NMR calculations expected in insulating materials. Therefore, such an effect should be considered when a high precision NMR shielding is computed for insulators. The exact value of this contribution depends a lot on the ionization state and the Ga-s charge. For instance, in GaF_3, the Ga^{3+} cation has approximately 3-times less Ga-s charge inside the atomic sphere than the neutral (or anionic) Ga in the digallides.

Considering the scaling of the paramagnetic component of σ_c, the value of the Ga-s PDOS at the Fermi level determines σ_c. This value, however, is related to the local atomic structure around Ga atoms. As shown in Figure 1, Ga(4b) in MGa_4 is coordinated by four equidistant Ga(5b) atoms that form slightly deformed tetrahedra. Ga(5b) have square pyramidal coordination by 5 Ga atoms (four Ga(4b) at the base and one Ga(5b) at the top). Ga in MGa_2 with M = Sr and Ba has three Ga neighbors that form flat triangles. The Ga-s character around the Fermi level originates from an overlap of Ga-p states localized at neighboring atoms. Therefore, "more spherical" local atomic environment, as it is for Ga(4b) in MGa_4 results in larger values of the Ga-s PDOS, and the "least spherical" triangular neighborhood results in the smallest Ga-s PDOS. This is what is seen in Figure 4 and delivers a simple qualitative relation between the type of local atomic structure and the resulting shielding.

As mentioned before, $BaGa_2$ stands out from the other gallides in showing a very large spin-dipolar component σ_{sd} to the spin part of the shielding. This can arise only from electrons with an orbital momentum $l > 0$, and for Ga, it is due to the Ga 4p ($l = 1$) states. To better understand this, we cast the second component of $\mathbf{B}_{hf}$ in eq 4 into a simple form:[39]

$$\mathbf{B}_{sd} \sim \sum_o \langle o|\frac{S(r)}{r^3}\left[l(l+1)\vec{s} - \frac{3}{2}(\vec{l}\cdot\vec{s})\vec{l} - \frac{3}{2}\vec{l}(\vec{s}\cdot\vec{l})\right]|o\rangle \tag{10}$$

where the sum runs over the occupied states. Since, we do not include spin−orbit coupling in our calculation we consider all states as pure spinors and eigenstates of s_z. For the spin up states, the Cartesian coordinates of $\mathbf{B}_{sd}$ are

$$B_{sd}^x \sim -\frac{3}{2}\sum_o \langle o|\frac{S(r)}{r^3}(l_z l_x + l_x l_z)|o\rangle$$

$$B_{sd}^y \sim -\frac{3}{2}\sum_o \langle o|\frac{S(r)}{r^3}(l_z l_y + l_y l_z)|o\rangle$$

$$B_{sd}^z \sim -\frac{3}{2}\sum_o \langle o|\frac{S(r)}{r^3}(l_x^2 + l_y^2 - 2l_z^2)|o\rangle \tag{11}$$

where we use the fact that $l(l+1)$ is an eigenvalue of $L^2 = l_x^2 + l_y^2 + l_z^2$. Without spin−orbit coupling B_{sd}^x and B_{sd}^y vanish. Due to the symmetry of the MGa_2 systems, the expectation value of l_x^2 and l_y^2 averaged over all occupied states are the same; therefore, B_{sd} can be further simplified into:

$$B_{sd}^z \sim -3\sum_o \langle o|\frac{S(r)}{r^3}(l_{x,y}^2 - l_z^2)|o\rangle \tag{12}$$

Contributions from spin down eigenstates will have opposite sign. Our systems are nonmagnetic, only slightly polarized by an external magnetic field and the total response is proportional to the integral of $-3\sum_o \langle o|\frac{S(r)}{r^3}(l_{x,y}^2 - l_z^2)|o\rangle$ around the Fermi level. Therefore, σ_{sd} should correlate with the difference of the partial $p_{x,y}$ and p_z DOS at ϵ_F. Figure 5 shows this difference for

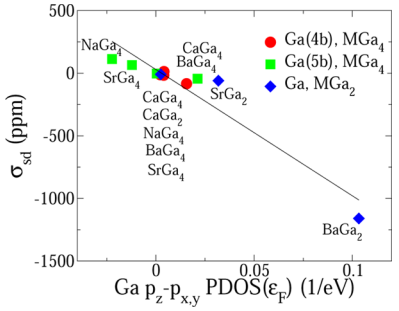

Figure 5. Relation of the spin-dipolar component σ_{sd} of the shielding to the difference of the Ga p_z and $p_{x,y}$ PDOS at ϵ_F collected for MGa_2 and MGa_4.

MGa_2 together with the resulting σ_{sd}. In fact, the differences in the PDOS and the resulting σ_{sd} are almost always very small except for $BaGa_2$ (please recall the previous discussion that the exact value of σ_{sd} for $BaGa_2$ is hard to calculate and depends on the smearing parameter). The Ga-p_z and $p_{x,y}$ PDOS for MGa_2 is shown in Figure 6. Only in the $BaGa_2$ case the Ga-p_z PDOS has

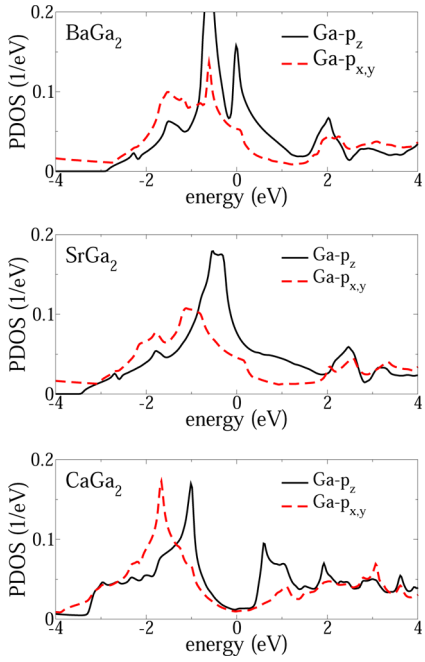

Figure 6. Ga p_z and $p_{x,y}$ PDOS for digallides.

DOI: 10.1021/acs.jpcc.6b11210
J. Phys. Chem. C 2017, 121, 753−760

a pronounced peak positioned exactly at the Fermi level and is much larger than the $p_{x,y}$ PDOS. The position of this Ga-p_z peak relative to ϵ_F, as well as to the Ga-$p_{x,y}$ PDOS is related to the Ga−Ga distance. We notice that for $CaGa_2$ this Ga-p_z feature is found well above the Fermi level and the Ga−Ga distance is largest and equal to 2.650 Å. On the other hand, for $SrGa_2$ the peak is placed below ϵ_F overlapping with Ga-$p_{x,y}$ and the Ga−Ga distance is smallest (2.511 Å). For $BaGa_2$, however, the Ga−Ga distance is intermediate (2.559 Å) leading to this extreme situation. The presence of such a sharp peak at ϵ_F results in a large dependence on the smearing temperature as observed for $BaGa_2$ and discussed before.

CONCLUSIONS

We have presented a detailed analysis of the computed Ga NMR shielding in various metallic gallides with different local Ga environment. Despite the fact that NMR calculations for metallic systems are quite challenging, our computed isotropic shielding correlates very well with the experimental shifts. The chemical trends are mainly due to the spin component of the response, which is dominated by the contact term for all cases except $BaGa_2$, which shows an unusually large spin-dipolar component. The relation between the local atomic structure and the isotropic shielding can be understood by looking at the value of the s-PDOS at the Fermi level. The Ga character of the bands close to ϵ_F are dominated by the 4p orbitals and the Ga-4s character develops due to the overlap with the neighbors, which is sensitive to the local atomic structure.

The response of the 4s wave functions to an external magnetic field leads in metals to a paramagnetic response due to a reoccupation of spin up and down states. However, when the s-PDOS at the Fermi level is small, a diamagnetic response of the spin contact term can be observed. It has its origin in a spin-splitting of all valence s-states (not just at ϵ_F) leading to a contraction/expansion of the corresponding 4s radial wave functions and a resulting positive spin-density at the nucleus. This non-negligible effect is present even in an insulator, although it has been ignored in the literature so far. The important message here is that only the part of the spin component of the shielding related to the reoccupation of the spin up and down eigenstates shows a linear scaling relation to the s-PDOS, but not the total contact term.

Our calculations identify also a large spin dipolar contribution for $BaGa_2$. This component develops due to a large difference between the p_z and $p_{x,y}$-PDOS at the Fermi level. The peculiar PDOS occurs for the specific Ga−Ga distance in the Ga honeycomb-like layer present in $BaGa_2$.

AUTHOR INFORMATION

Corresponding Author

*E-mail: rolask@ihpc.a-star.edu.sg.

ORCID

Khoong Hong Khoo: 0000-0002-4628-1202

Notes

The authors declare no competing financial interest.

ACKNOWLEDGMENTS

The authors acknowledge the use of computational resources of ACRC and NSCC, Singapore. This work was supported by the Project No. SFB-F41 (ViCoM) of the Austrian Science Fund.

REFERENCES

(1) Laskowski, R.; Blaha, P. *J. Phys. Chem. C* **2015**, *119*, 731−740.
(2) Laskowski, R.; Blaha, P. *Phys. Rev. B: Condens. Matter Mater. Phys.* **2012**, *85*, 245117−245123.
(3) Charpentier, T. *Solid State Nucl. Magn. Reson.* **2011**, *40*, 1.
(4) d'Avezac, M.; Marzari, N.; Mauri, F. *Phys. Rev. B: Condens. Matter Mater. Phys.* **2007**, *76*, 165122−165134.
(5) Laskowski, R.; Blaha, P. *J. Phys. Chem. C* **2015**, *119*, 19390−19396.
(6) Zintl, E. *Naturwissenschaften* **1929**, *17*, 782−783.
(7) Fornasini, M. L.; Pani, M. *Acta Crystallogr., Sect. C: Cryst. Struct. Commun.* **1986**, *42*, 394−396.
(8) Fornasini, M. L. *Acta Crystallogr., Sect. C: Cryst. Struct. Commun.* **1983**, *39*, 943−946.
(9) Haarmann, F.; Koch, K.; Grüner, D.; Schnelle, W.; Pecher, O.; Cardoso-Gil, R.; Borrmann, H.; Rosner, H.; Grin, Y. *Chem. - Eur. J.* **2009**, *15*, 1673−1684.
(10) Haarmann, F.; Koch, K.; Jeglič, P.; Pecher, O.; Rosner, H.; Grin, Y. *Chem. - Eur. J.* **2011**, *17*, 7560−7568.
(11) Sharma, B. D.; Donohue, J. Z. *Kristallogr.* **1962**, *117*, 293−300.
(12) Bruzzone, G.; Fornasini, M. L.; Merlo, F. *J. Less-Common Met.* **1989**, *154*, 67−77.
(13) Iandelli, A. *Z. Anorg. Allg. Chem.* **1964**, *330*, 221−232.
(14) Momma, K.; Izumi, F. *J. Appl. Crystallogr.* **2011**, *44*, 1272−1276.
(15) Pecher, O.; Mausolf, B.; Lamberts, K.; Oligschläger, D.; Niewieszol (née Merkens), C.; Englert, U.; Haarmann, F. *Chem. - Eur. J.* **2015**, *21*, 13971−13982.
(16) Pecher, O.; Mausolf, B.; Peters, V.; Lamberts, K.; Korthaus, A.; Haarmann, F. *Chem. - Eur. J.* **2016**, *22*, 1−11.
(17) Goebel, T.; Ormeci, A.; Pecher, O.; Haarmann, F. *Z. Anorg. Allg. Chem.* **2012**, *638*, 1437−1445.
(18) Abragam, A. *Principles of Nuclear Magnetism*; Oxford University Press: Oxford, NY, 1961.
(19) Slichter, C. P. *Principles of Magnetic Resonance*, 3rd enlarged and updated ed.; Springer-Verlag: Berlin, Heidelberg, NY, 1990.
(20) Knigh, W. D.; Kobayashi, S. In *Encyclopedia of Nuclear Magnetic Resonance*; Grant, D. M., Harris, R. K., Eds.; John Wiley & Sons: Chichester, New York, Brisbane, Toronto, Singapore, 1996; Chapter Knight Shift, pp 2672−2679.
(21) Knight, W. D.; Kobayashi, S.-I. In *Enzyclopedia of Magnetic Resonance*; Harris, R. K., Wasylishen, R. E., Eds.; John Wiley: Chichester, 2007.
(22) Haarmann, F. In *Enzyclopedia of Magnetic Resonance*; Harris, R. K., Wasylishen, R. E., Duer, M. J., Eds.; John Wiley: Chichester, West Sussex, 2011.
(23) Mauri, F.; Pfrommer, B. G.; Louie, S. G. *Phys. Rev. Lett.* **1996**, *77*, 5300−5303.
(24) Pickard, C. J.; Mauri, F. *Phys. Rev. B: Condens. Matter Mater. Phys.* **2001**, *63*, 245101−245114.
(25) Yates, J. R.; Pickard, C. J.; Mauri, F. *Phys. Rev. B: Condens. Matter Mater. Phys.* **2007**, *76*, 024401−024412.
(26) Singh, D. J.; Nordström, L. *Planewaves, Pseudopotentials and the LAPW Method*, 2nd ed; Springer: New York, 2006.
(27) Blaha, P.; Schwarz, K.; Madsen, G. K. H.; Kvasnicka, D.; Luitz, J. *WIEN2k, An Augmented Plane Wave Plus Local Orbitals Program for Calculating Crystal Properties, User's Guide*; Vienna University of Technology, 2001.
(28) Laskowski, R.; Blaha, P. *Phys. Rev. B: Condens. Matter Mater. Phys.* **2012**, *85*, 035132−035144.
(29) Laskowski, R.; Blaha, P. *Phys. Rev. B: Condens. Matter Mater. Phys.* **2014**, *89*, 014402−014409.
(30) Gregor, T.; Mauri, F.; Car, R. *J. Chem. Phys.* **1999**, *111*, 1815−1822.
(31) Blügel, S.; Akai, H.; Zeller, R.; Dederichs, P. H. *Phys. Rev. B: Condens. Matter Mater. Phys.* **1987**, *35*, 3271−3283.
(32) Perdew, J. P.; Burke, K.; Ernzerhof, M. *Phys. Rev. Lett.* **1996**, *77*, 3865−3868.
(33) Harms, W.; Wendorff, M.; Röhr, C. *Z. Naturforsch.* **2006**, *62b*, 177.

DOI: 10.1021/acs.jpcc.6b11210
J. Phys. Chem. C 2017, 121, 753−760

(34) Laskowski, R.; Blaha, P.; Tran, F. *Phys. Rev. B: Condens. Matter Mater. Phys.* **2013**, *87*, 195130−195138.
(35) Becke, A. D.; Johnson, E. R. *J. Chem. Phys.* **2006**, *124*, 221101−221105.
(36) Mason, J. *Multinuclear NMR*; Kluwer Academic/Plenum Publishers: Buckinghamshire, 1987.
(37) Slichter, C. P. *Principles of Magnetic Resonance*, 3rd ed; Springer: Berlin, 1990.
(38) Schwarz, K.; Mohn, P. *J. Phys. F: Met. Phys.* **1984**, *14*, L129.
(39) Abragam, A.; Bleaney, B. *Electron Paramagnetic Resonance of Transition Ions*; Clarendon Press: Oxford, 1970.

DOI: 10.1021/acs.jpcc.6b11210
J. Phys. Chem. C 2017, 121, 753−760